Mechanics of Materials 9 (1990) 83–91
Elsevier

ON TOUGHENING BY MICROCRACKS

David K.M. SHUM and John W. HUTCHINSON
Division of Applied Sciences, Harvard University, Cambridge, MA 02138, U.S.A.

Received 11 November 1989

This study examines the phenomenon of microcrack toughening under the premise that toughening must entail mutual shielding of the main crack *and* the microcracks. Maximum toughening corresponds to the macrocrack/microcrack configuration that minimizes the maximum energy release rate (or stress intensity factor) among the various crack tips. Explicit results for the maximum toughening achievable and the corresponding optimal configuration are presented for a plane strain model of a macrocrack in the presence of either one or two microcracks.

1. Introduction

Some brittle single phase polycrystalline materials display a macroscopic fracture energy which is many times the fracture energy for cleavage of the single crystals or the fracture energy of grain boundary separation. Thus, even in the absence of any plastic deformation, the polycrystal can be much tougher than its constituent crystals or its grain boundaries. A number of toughening mechanisms have been suggested to account for this rather counterintuitive phenomenon. Each mechanism proposed is connected one way or another to heterogeneity on the scale of the grains. They include crack deflection, microcrack shielding, and crack bridging by uncracked grains. Quantitative toughening predictions for these mechanisms are not yet firmly established and a consensus on conditions when one mechanism is expected to dominate has not been reached.

This paper focuses on microcracking and addresses the question of the maximum toughening which can be expected from this mechanism. Considerable theoretical work has recently been devoted to the phenomenon of microcrack shielding in brittle materials. Some studies approach the problem on a continuum scale (Evans and Faber, 1980; Hoagland and Embury, 1980; Hutchinson, 1987; Ortiz, 1988) where a profusion of microcracks are imagined to participate in the process of shielding the main crack. Other studies (Rose, 1986; Rubinstein, 1986; Hori and Nemat-Nasser, 1987; Kachanov, 1987; Montagut and Kachanov, 1988; Gong and Horii, 1989) treat the microcracks as discrete entities interacting with the main crack tip. There are two potential contributions to toughening from microcracking. One is crack tip stress redistribution due to the release of residual stress when a microcrack is nucleated. This contribution is rather similar to plastic deformation at a crack tip in a metal or to dilatational transformation at the tip of a crack in a ceramic. The residual stress is present and varies from grain to grain when the crystals have thermal-expansion anisotropy. The other contribution results in stress redistribution at the main tip due to microcracking in the absence of residual stress. In the continuum approach this redistribution results due to the lowering of the stiffness of the microcracked material. In the discrete approach the redistribution occurs directly from the interaction of the microcracks with the main crack. It is this latter contribution which is of concern in this paper. The contribution due to release of residual stress is reasonably well in hand (Hutchinson, 1987) and does not present any major computational difficulties.

Specifically, in this paper, the interaction between one or two microcracks located near the tip of a macrocrack is considered. Optimal configura-

tions are found which minimize the maximum energy release rates for *all* the crack tips involved. Although the outcome of a highly idealized model, these results supply insight into the maximum amount of toughening which can be expected from this contribution of microcracking. Prior work has primarily focussed on shielding of the main crack with no regard for any attendant amplification of the energy release rates of the microcracks. A toughening enhancement requires the *mutual shielding* of the main tip and the tips of the microcracks, otherwise crack advance will occur from one of the microcracks. This is the motivation for the search for the configuration with the lowest possible maximum energy release rate of all the crack tips involved.

This study is highly idealized in that attention is limited to plane strain cracks in an isotropic elastic solid. Microcracks in a brittle polycrystal usually nucleate on a grain boundary facet and arrest at a junction, or they may form on a crystal cleavage plane and arrest at the first grain boundary they encounter. In either case, the heterogeneity at the scale of the grains sets the size and orientation of the microcracks, and nucleation is usually assisted by residual stresses. Nevertheless, the results of this study do isolate an essential aspect of the interaction between a macrocrack and microcracks as it pertains to toughening.

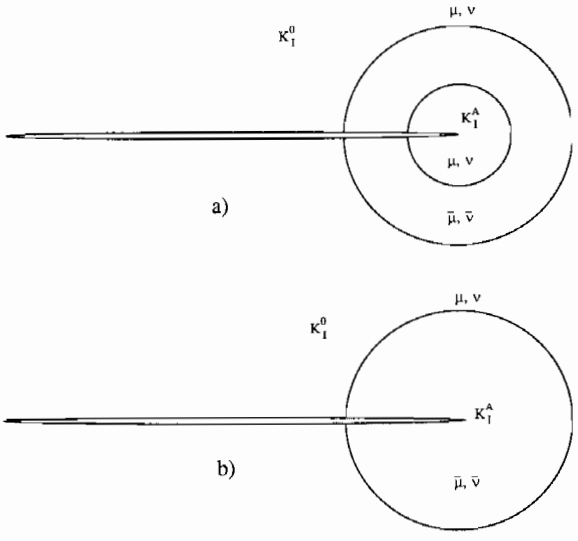

Fig. 1. Zone of reduced stiffness surrounding the tip of a semi-infinite crack: (a) annular reduced stiffness zone, and (b) reduced stiffness zone extends all the way to crack tip.

A rationale for limiting attention to the one or two microcracks nearest the main crack tip can be found from both continuum and discrete interaction theories. Calculations using large arrays of discrete microcracks interacting with the macrocrack (Montagut and Kachanov, 1988) suggest that the locations of the nearest microcracks largely determine whether shielding or antishielding occurs. The details of the distribution of the microcracks outside the immediate tip region appear to be less important. The same conclusion can be drawn from continuum studies of the effect of zones of less stiff material surrounding a macrocrack tip (Hutchinson, 1987). Consider the semi-infinite crack in Fig. 1a which is surrounded by an annular circular zone with a reduced shear modulus $\bar{\mu}$ and an altered Poisson's ratio $\bar{\nu}$. The crack is subject to a remote mode I loading characterized by K_I^0, and the stress intensity factor at the tip within the annular zone (with modulus μ and ν) is K_I^A. To lowest order in the differences in moduli, $\bar{\mu} - \mu$, and Poisson's ratio, $\bar{\nu} - \nu$,

$$K_I^A = K_I^0 \tag{1.1}$$

In other words, the annular zone of less stiff material surrounding the tip has neither a shielding nor an antishielding effect to lowest order. If the less stiff zone extends all the way to the tip such that the tip lies in the less stiff material, as shown in Fig. 1b, the crack tip stress intensity factor is altered according to

$$\frac{K_I^A}{K_I^0} = 1 - \frac{5}{8(1-\nu)}\left[\frac{\mu}{\bar{\mu}} - 1\right] + \frac{3}{4(1-\nu)}\left[\bar{\nu}\frac{\mu}{\bar{\mu}} - 1\right] \tag{1.2}$$

to lowest order in the moduli and Poisson's ratio differences (Hutchinson, 1987). Thus, it is the inner core of less stiff material, as opposed to the surrounding annular region, which mainly influences the stress level at the crack tip. Note also that the size of the circular zone does not enter into (1.2). Increasing the zone size does not alter the shielding.

2. Formulation of the problem

Consider the configuration in Fig. 2a where a single microcrack of length $2a$ is positioned near the tip of the main crack. The tip of the main crack is subject to a mode I stress intensity factor K_I^0 in the absence of the microcrack. When the size and distance of the microcrack from the tip is very small compared to the length of the macrocrack, one can consider an asymptotic problem where the semi-infinite main crack is remotely stressed consistent with the classical mode I crack tip field

$$\sigma_{ij} = \frac{K_I^0}{\sqrt{2\pi r}} \tilde{\sigma}_{ij}(\theta) \tag{2.1}$$

where (r, θ) are plane polar coordinates. The microcrack is arbitrarily positioned as characterized by the two angles, α and ω, and the distance, d, of its center from the main tip. Let

$$\mathcal{G}_0 = K_I^{0^2} \frac{(1-\nu^2)}{E} \tag{2.2}$$

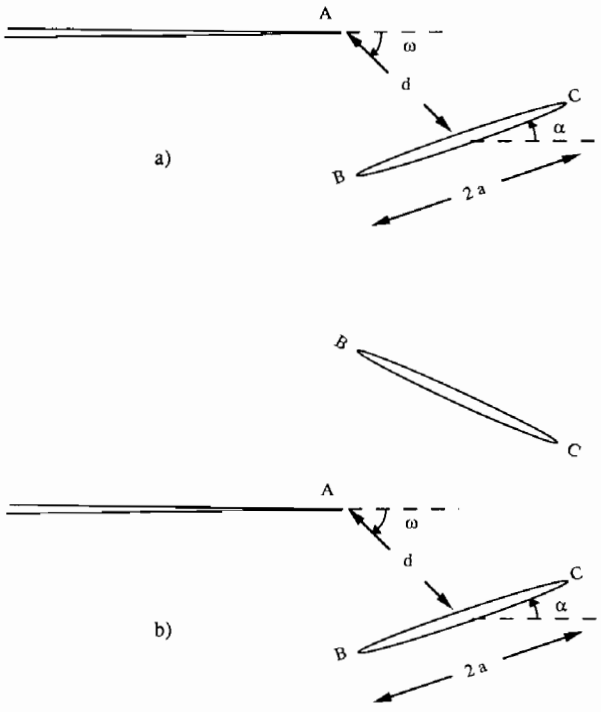

Fig. 2. Macrocrack/microcrack configurations: (a) one microcrack and (b) two symmetric microcracks.

be the energy release rate of the main tip in the absence of the microcrack, where E is Young's modulus and ν is Poisson's ratio. It will be referred to as the applied energy release rate. Denote the energy release rates of the three tips in the interaction problem in Fig. 2a by $\mathcal{G}_A$, $\mathcal{G}_B$ and $\mathcal{G}_C$. By dimensional considerations and the fact that a linear, plane strain problem is being analyzed, one concludes that

$$\mathcal{G}_A/\mathcal{G}_0 = f(d/a, \alpha, \omega) \tag{2.3}$$

with a functional dependence on the same variables for $\mathcal{G}_B/\mathcal{G}_0$ and $\mathcal{G}_C/\mathcal{G}_0$. Similarly the mode I or mode II stress intensity factor of any of the three tips must depend on the same three nondimensional position variables according to

$$K/K_I^0 = g(d/a, \alpha, \omega) \tag{2.4}$$

Thus, a small microcrack close to the tip has the same effect as a large microcrack farther from the tip with the same d/a ratio. More to the point for application to polycrystals, the influence of a microcrack of fixed size (e.g. the size of a grain facet) is larger the closer it is to the macrocrack tip. This observation is clearly related to the special role of the microcracks nearest the tip noted in the Introduction.

The two-microcrack configuration in Fig. 2b will also be considered. In this case the cracks will be restricted to be symmetrically positioned with respect to the semi-infinite main crack. Thus, by symmetry, only results for tips A, B and C need to be considered.

The solution to the interaction problem is obtained by numerical solution to an exact integral equation formulation similar to that used by Hori and Nemat-Nasser (1987), Kachanov (1987), and Gong and Horii (1989). This formulation and the reduction for numerical analysis is given in the Appendix. The solution procedure leads to highly accurate results for the stress intensity factors and energy release rates. High accuracy is needed for the present minimization problem. Various approximate solutions, or solution procedures, have been proposed for the interaction problem. These approximations all tended to lose accuracy when $d/a < 1$ and the microcrack is located off the plane of the main crack as in Fig. 2a. In particu-

lar, they have large errors for the optimal crack configurations reported in the next section.

Two minimax problems are considered in this paper:

Problem No. 1

Minimize the maximum of $(\mathcal{G}_A/\mathcal{G}_0, \mathcal{G}_B/\mathcal{G}_0, \mathcal{G}_C/\mathcal{G}_0)$ with respect to all admissible d/a, α and ω. Admissible values of the position variables are those for which the cracks do not intersect.

Problem No. 2

Minimize the maximum of $(K_I^A/K_I^0, K_I^B/K_I^0, K_I^C/K_I^0)$ with respect to all admissible d/a, α and ω.

Solutions to the minimax problems are carried out using the Least Pth algorithm (Bandler and Charalambous, 1972) coupled with a Simplex search method (Press et al., 1986). In the terminology of optimization, the objective function to be minimized is either the maximum energy release rate or the maximum mode I stress intensity factor among all the crack tips.

3. Solutions, optimal solutions and inferences

As an illustrative example, consider the special subset of configurations for the two-microcrack problem wherein the microcracks are parallel to the main crack ($\alpha = 0$) and d/a is fixed at the value 1.2. The dependence of the energy release rates of the tips on ω is shown in Fig. 3. When the microcrack is ahead of the macrocrack ($\omega < 60^0$) the energy release rate of the macrocrack tip is amplified above the applied value. Within this subset of configurations, the maximum shielding of the main tip A occurs when $\omega \cong 130°$ with $\mathcal{G}_A = 0.325$. However, in this configuration the energy release rate of tips C of the microcracks is larger than that of the main crack. Maximum mutual shielding (i.e. the minimum maximum energy release rate) in this subset of configurations occurs when $\omega \cong 140°$ with $\mathcal{G}_A = \mathcal{G}_C$.

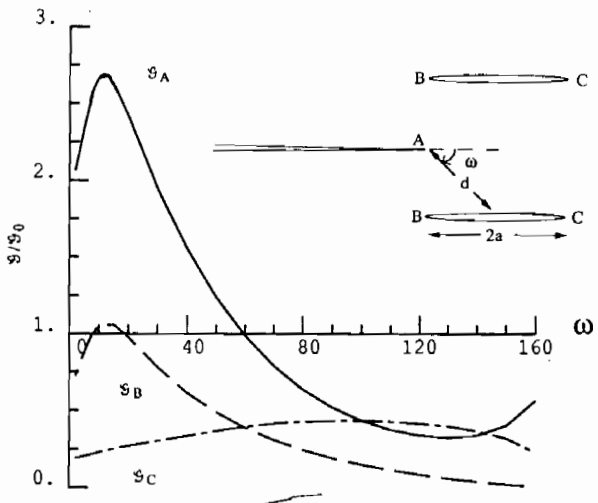

Fig. 3. Variation of energy release rates with ω for $d/a = 1.2$ and $\alpha = 0$.

Table 1
Optimal solutions for one- and two-microcrack configurations (objective function minimized)

Optimal solution	One microcrack		Two microcracks	
	G	K_I	G	K_I
ω	145.8	149.9	147.9	150.4
α	27.0	25.1	27.4	24.3
d/a	1.02	1.01	1.02	1.02
$\mathcal{G}_A$	0.468	0.429	0.289	0.246
$\mathcal{G}_B$	0.001	0.001	0.001	0.000
$\mathcal{G}_C$	0.468	0.502	0.289	0.312
K_I^A	0.683	0.652	0.538	0.496
K_I^B	0.031	0.025	0.023	0.020
K_I^C	0.623	0.653	0.475	0.495
K_{II}^A	0.042	−0.056	0.000	0.000
$*K_{II}^B$	0.017	0.007	−0.003	0.008
$*K_{II}^C$	0.283	0.276	0.252	0.259

* Bottom crack.

The results of the solutions to the two minimax problems over the full range of admissible d/a, α and ω are presented in Table 1. The optimal configurations are shown in Fig. 4. Note that the differences between the optimal solutions and configurations are very small. Moreover, the optimal position parameters characterizing the one-microcrack problem are almost the same as for the two-microcrack problem. For Problem No. 1 where the objective function is based on the energy release rate the optimal solution gives

$$\mathcal{G}_A/\mathcal{G}_0 = \mathcal{G}_C/\mathcal{G}_0 = 0.468 \quad \text{(one microcrack)} \tag{3.1}$$

$$\mathcal{G}_A/\mathcal{G}_0 = \mathcal{G}_C/\mathcal{G}_0 = 0.289 \quad \text{(two microcracks)} \tag{3.2}$$

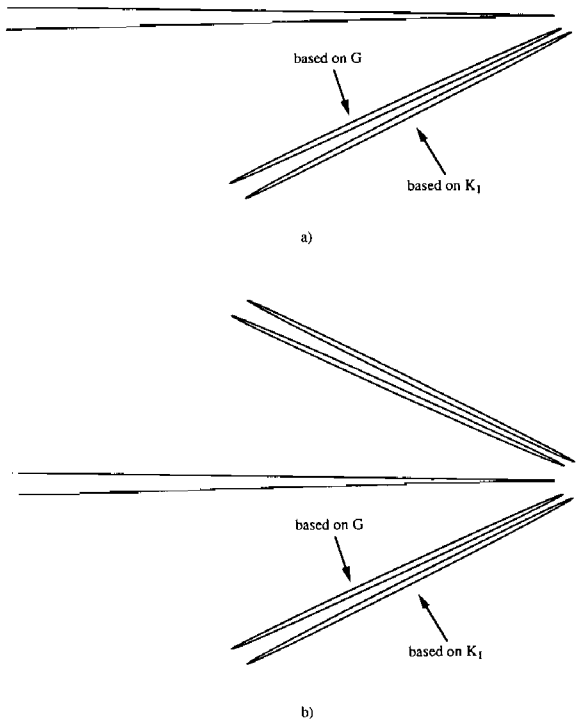

Fig. 4. Optimal one- and two-microcrack configurations.

The objective function space is relatively flat in the neighborhood of the minimum solution. This holds true for each of the two objective functions and for the one- or two-microcrack problems. Thus there is a range of configurations about those listed in Table 1 for which the values of $\mathcal{G}_A$ and $\mathcal{G}_C$ are essentially the optimal values. For the same reason, the values of position variables for the optimal configurations are less accurate than the optimal values of the objective function, i.e. $\mathcal{G}$ or K.

The optimal results are not entirely unexpected. Consider, for example, the configuration in the insert in Fig. 5 where a single microcrack is parallel to the main crack and the two lead tips, A and C, are equally extended. The variation of the energy release rates of the three tips with c/a is shown. As can be understood from elementary considerations, the applied energy release rate becomes equally partitioned between each of the lead tips when $c/a \ll 1$ and

$$\mathcal{G}_A/\mathcal{G}_0 \to \mathcal{G}_C/\mathcal{G}_0 \to 1/2 \quad \text{as } c/a \to 0 \tag{3.3}$$

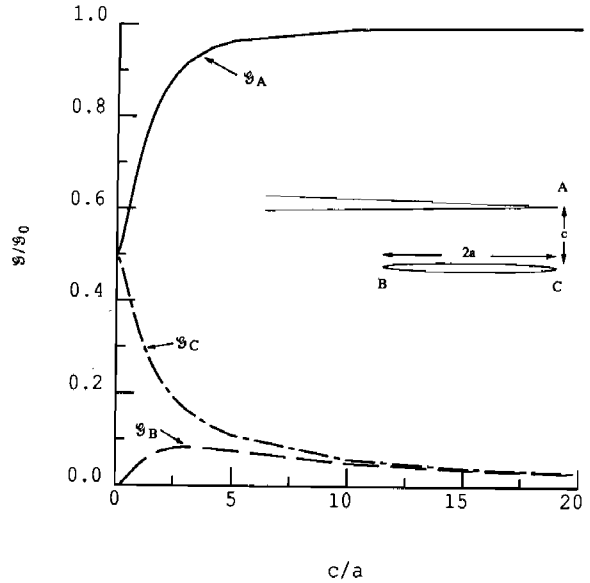

Fig. 5. Variation of energy release rates with c/a for a single microcrack parallel to main crack with aligned leading tips.

This arrangement is not far from optimal for the one microcrack case.

The two-microcrack case is not so easily understood. The analogous arrangement of two parallel microcracks has a variation of energy release rates

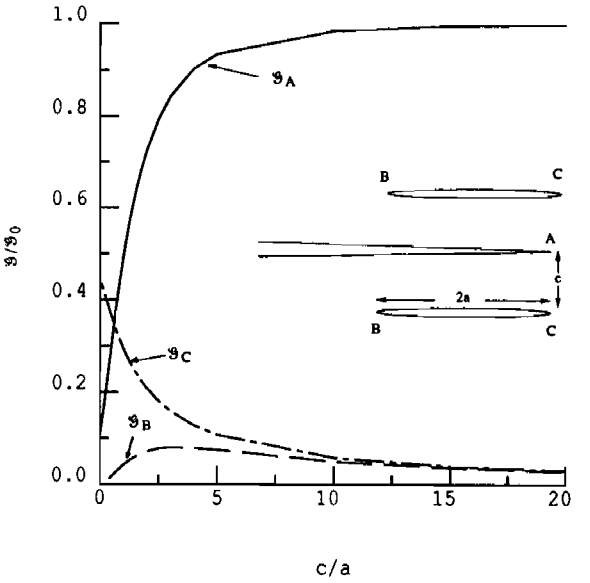

Fig. 6. Variation of energy release rates with c/a for two microcracks parallel to main crack with aligned leading tips.

shown in Fig. 6. In this case, the applied energy release rate is not equally partitioned as $c/a \to 0$. Instead the main tip is shielded such that

$$\mathcal{G}_A/\mathcal{G}_0 \cong 0.1 \quad \text{and} \quad \mathcal{G}_C/\mathcal{G}_0 \cong 0.45 \quad \text{as } c/a \to 0 \tag{3.4}$$

This configuration is quite far from optimal.

The optimal values of the mutually shielded tips in (3.1) and (3.2) suggest that the *largest* amount of microcrack toughening (excluding the contribution from the release of residual stress) that can be expected is 2 or 3 times the "intrinsic" toughness measured in surface energy units. That is, if crack advance of each of the tips is controlled by a critical value of energy release rate, $\mathcal{G}_{\text{CRIT}}$, then there exist one- or two-microcrack configurations for which the critical applied energy release rate, $\mathcal{G}_0$, is 2 or 3 times $\mathcal{G}_{\text{CRIT}}$. Whether optimal, or near optimal, configurations can actually control the overall toughness in a statistical sense along a crack front is an open issue.

The above conclusion is not only tempered by the fact that the calculation is a two dimensional one. As discussed in the Introduction, it is also premised on the assumption that shielding is dominated by the microcracks closest to the tip. In addition, the assumption of an "intrinsic" toughness, $\mathcal{G}_{\text{CRIT}}$, is obviously a simplification. Local conditions such as geometry, elastic anisotropy mismatches, and residual stresses at a grain boundary junction or grain boundary where a tip has arrested will influence the critical energy release rate for that tip at that location. The manner in which all these influences work to establish the polycrystalline toughness is extremely complex and difficult to model. The present results, though highly idealized, provide a reference for the effect of microcracking on toughness, excluding the contributions from the release of residual stress.

Acknowledgements

This work was supported by the Materials Research Laboratory (Grant NSF-DMR-86-14003) and DARPA University Research Initiative (Subagreement P.O. #VB38639-0 with the University of California, Santa Barbara, ONR Prime Contract N00014-86-K-0753) and the Division of Applied Sciences, Harvard University.

References

Bandler, J.W. and C. Charalambous (1972), Practical Least Pth optimization of networks, *IEEE Trans. Microwave MTT-20,* 834.

Evans, A.G. and K.T. Faber (1980), Toughening of ceramics by circumferential microcracking, *J. Amer. Ceram. Soc. 64,* 394.

Gong, S. and H. Horii (1989), General solution to the problem of microcracks near the tip of a main crack, *J. Mech. Phys. Solids 37,* 27.

Hoagland, R.G. and J.D. Embury (1980). A treatment of inelastic deformation around a crack tip due to microcracking, *J. Amer. Ceram. Soc. 63,* 404.

Hori, M. and S. Nemat-Nasser (1987), Interacting micro-cracks near the tip in the process zone of a macro-crack, *J. Mech. Phys. Solids 35,* 601.

Hutchinson, J.W. (1987), Crack tip shielding by micro-cracking in brittle solids, *Acta Metall. 35,* 1605.

Kachanov, M. (1987), Elastic solids with many cracks: A simple method of analysis, *Int. J. Solids Struct. 23,* 23.

Montagut, E. and M. Kachanov (1988), On modelling a microcracked zone by weakened elastic material and on statistical aspects of crack–microcrack interactions, *Int. J. Fract. 37,* R55.

Ortiz, M., (1988), Microcrack coalescence and macroscopic crack growth initiation in brittle solids, *Int. J. Solids Struct. 24, 231.*

Press, W.H., B.P. Flannery, S.A. Teukolsky and W.T. Vetterling (1986), *Numerical Recipes,* Cambridge University Press.

Rose, L.R.F. (1986), Microcrack interaction with a main crack, *Int. J. Fract. 31,* 233.

Rubinstein, A.A. (1986), Macrocrack–microcrack interactions, *J. Appl. Mech. 53,* 505.

Tada H., P.C. Paris and G.R. Irwin (1985), *Handbook for Stress Analysis of Cracks,* Del Research, 2nd edn.

Appendix

Macrocrack / microcrack interaction solution

The solution methodology is illustrated for the case of a none-microcrack system involving a semi-infinite crack and a microcrack of length $2a$ within an infinite body subject to remote loading as shown in Fig. A.1. Following the procedures in

Hori and Nemat-Nasser, 1987; Kachanov, 1987; Gong and Horii, 1989) the total problem in Fig. A.1 is decomposed into three subproblems where each subproblem contains only one crack. Based on linear superposition principles, the stress intensity factors at the various crack tips in the total problem are found by summing the stress intensity factor contributions of the corresponding crack tips in the three subproblems. The macrocrack/microcrack interaction solution method involves constructing the integral equations governing pseudo-tractions $\tau_\beta^A(\rho)$ and $\tau_\beta^B(\eta)$ on the faces of the two cracks in subproblems 2 and 3. Here ρ is the lineal coordinate along the semi-infinite crack wake with $\rho = 0$ at the tip, and η is the lineal coordinate along the microcrack face, where $\eta = 0$ is midpoint of the microcrack.

In subproblem 1 the semi-infinte crack is subject to the same remote loadings as that found in the total problem. The resultant traction along the line segment BC has a component along the direction of BC denoted as $\sigma_1^*(\eta)$ and a component perpendicular to BC denoted as $\sigma_2^*(\eta)$. The location of the line segment BC corresponds to the location of the microcrack in the total problem.

In subproblem 2 the stress field within the infinite body is due to a traction distribution along the semi-infinite crack faces with a shear

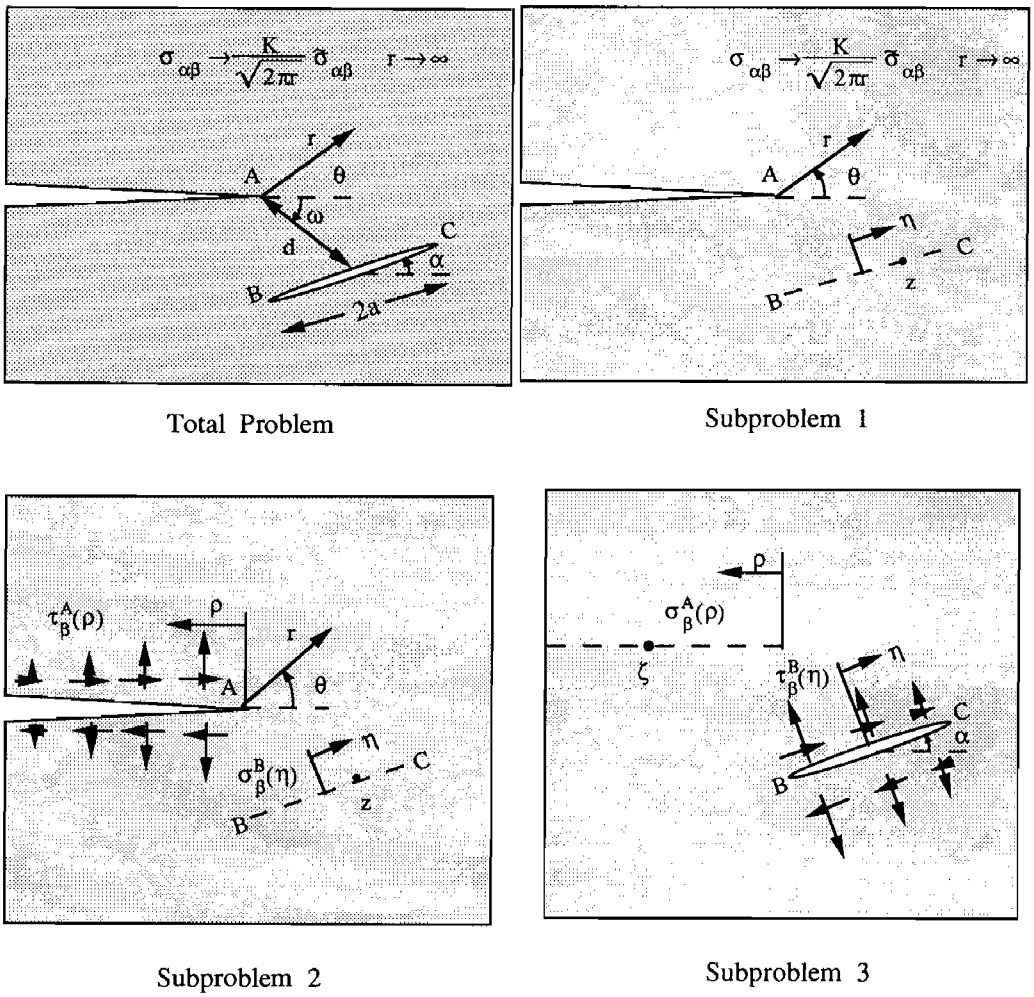

Total Problem

Subproblem 1

Subproblem 2

Subproblem 3

Fig. A.1. Decomposition of macrocrack/microcrack interaction problem into three subproblems.

component $\tau_1^A(\rho)$ and a normal component $\tau_2^A(\rho)$. The traction distribution $\tau_\beta^A(\rho)$ is needed to maintain traction-free boundary condition along the semi-infinite crack faces in the total problem, the magnitudes of its components to be determined as part of the solution to the total problem. The resultant traction along the line segment BC has components $\sigma_\beta^B(\eta)$.

Similarly, in subproblem 3 the stress field within the infinite body is due to a traction distribution along the microcrack faces with a shear component $\tau_1^B(\eta)$ and a normal component $\tau_2^B(\eta)$. The resultant traction along the semi-infinite line segment has components $\sigma_1^A(\rho)$ and $\sigma_2^A(\rho)$ along directions that are parallel and perpendicular to the line segment.

Solution of the total problem is found by requiring the unknown tractions $\tau_\beta^A(\rho)$ and $\tau_\beta^B(\eta)$ in the subproblems to result in traction-free crack faces in the total problem such that

$$\begin{aligned} &\sigma_\beta^A(\rho) + \tau_\beta^A(\rho) = 0 \qquad \text{for } 0 \leqslant \rho < \infty \\ &\sigma_\beta^B(\eta) + \tau_\beta^B(\eta) = -\sigma_\beta^*(\eta) \quad \text{for } -a < \eta < a \end{aligned} \tag{A.1}$$

From this point on our procedure departs somewhat from those in (Hori and Nemat-Nasser, 1987; Kachanov, 1987; Gong and Horii, 1989).

Subproblem 1

Let the applied K field for the *total* problem be expressed in complex form such that

$$K = K_I^0 + \mathrm{i}K_{II}^0 \tag{A.2}$$

where $\mathrm{i} = \sqrt{-1}$ and K_{II}^0 has been included. The stresses $\sigma_\beta^*(\eta)$ then take the form

$$\begin{aligned} \sigma_2^* &= \mathrm{Re}[Z + \mathrm{i}Y] \\ \sigma_1^* &= \mathrm{Re}[Y] \end{aligned} \tag{A.3}$$

where

$$\begin{aligned} Y &= -(\mathrm{Im}(Z) + yZ')e^{\mathrm{i}2\alpha} \qquad (\,)' \equiv \frac{\mathrm{d}}{\mathrm{d}z} \\ Z &= \frac{\bar{K}}{\sqrt{2\pi z}} \end{aligned} \tag{A.4}$$

Here, $\bar{K}$ denotes the complex conjugate of K and z is the complex variable denoting the position of the point on BC.

Subproblem 2

The resultant stresses $\sigma_\beta^B(\eta)$ due to the pseudo-traction $\tau_\alpha^A(\rho)$ are defined as

$$\sigma_\beta^B(\eta) = -\int_0^\infty K_{\beta\alpha}^A(\eta;\, \rho)\tau_\alpha^A(\rho)\, \mathrm{d}\rho \tag{A.5}$$

where $K_{\beta\alpha}^A(\eta;\, \rho)$ is the β component of the resolved stresses on the line segment BC at location η due to a pair of unit line loads applied on the semi-infinite crack faces at location ρ. Here the repeated indice α is to be summed from 1 to 2. Explicit expressions for $K_{\beta\alpha}^A$ can be derived from results in (Tada et al., 1985). For numerical evaluation of the integrals in (A.5) let

$$\tau_\alpha^A(u) = (1-u)^2 \sum_{j=1}^{N} A_{j\alpha}U_{j-1}(u) \quad \frac{\rho}{a} = \frac{1+u}{1-u} \tag{A.6}$$

where $U_{j-1}(u)$is Chebyshev polynomial of the second kind of degree $j-1$ and u is the nondimensional distance variable defined such that $-1 \leqslant u \leqslant 1$. For admissible microcrack configurations where the microcrack and the semi-infinite crack do not overlap, (A.5) can be integrated exactly in closed form giving

$$\sigma_\beta^B(\eta) = \sum_{j=1}^{N} A_{j\alpha}F_{\beta\alpha}(\eta) \tag{A.7}$$

Subproblem 3

The resultant stresses $\sigma_\beta^A(\rho)$ due to the pseudo-traction $\tau_\alpha^B(\eta)$ are similarly defined as

$$\sigma_\beta^A(\rho) = -\int_{-a}^{a} K_{\beta\alpha}^B(\rho;\, \eta)\tau_\alpha^B(\eta)\, \mathrm{d}\eta \tag{A.8}$$

Explicit expressions for $K_{\beta\alpha}^B$ can also be derived from results in (Tada et al., 1985). For numerical evaluation of the integrals in (A.8) let

$$\tau_\alpha^B(w) = \sum_{j=1}^{N} B_{j\alpha}U_{j-1}(w) \quad \text{with } w = \frac{\eta}{a} \tag{A.9}$$

Again, for admissible microcrack configurations (A.8) can be integrated exactly in closed form giving

$$\sigma_\beta^A(\rho) = \sum_{j=1}^{N} B_{j\alpha} G_{\beta\alpha}(\rho) \tag{A.10}$$

Stress intensity factors

Substitution of (A.3, A.6, A.7, A.9 and A.10) into (A.1) results in a system of equations which are linear in the $4N$-unknowns, $A_{j\alpha}$ and $B_{j\alpha}$, and which have an explicit, closed form dependence on ρ and η. Each of the four equations (A.6, A.9) are collocated at N points denoted as t_k where

$$U_N(t_k) = 0, \quad t_k = \cos\left(\frac{k\pi}{N+1}\right), \quad k = 1, \ldots, N \tag{A.11}$$

The stress intensity factors at the semi-infinite crack tip are found by combining the stress intensity factor contributions from subproblems 1 and 2 such that (Tada et al., 1985)

$$K_\xi^A = K_\xi^0 - \sqrt{\frac{2a}{\pi}} \int_0^\infty \frac{1}{\sqrt{u}} \tau_\xi^A(u)\, du \tag{A.12}$$

where K_ξ^0 are the magnitudes of the applied mode I and II stress intensity factors. The integrals in (A.12) can be integrated exactly in closed form giving

$$K_\xi^A = K_\xi^\infty + 2\sqrt{2\pi a} \sum_{j=1}^{N} (-1)^j A_{j\xi} \tag{A.13}$$

The stress intensity factors at the microcrack tip C due to $\tau_\xi^B(\eta)$ take the form (Tada et al., 1985)

$$K_\xi^C = -\sqrt{\frac{a}{\pi}} \int_{-1}^{1} \sqrt{\frac{1+w}{1-w}}\, \tau_\xi^B(\eta)\, d\eta \tag{A.14}$$

which can be integrated exactly in closed form giving

$$K_\xi^C = -\sqrt{\pi a} \sum_{j=1}^{N} B_{j\xi} \tag{A.15}$$

Similarly, the stress intensity factors at the microcrack tip B take the form

$$K_\xi^B = -\sqrt{\frac{a}{\pi}} \int_{-1}^{1} \sqrt{\frac{1-w}{1+w}}\, \tau_\xi^B(\eta)\, d\eta \tag{A.16}$$

which can also be integrated exactly in closed form giving

$$K_\xi^B = \sqrt{\pi a} \sum_{j=1}^{N} (-1)^j B_{j\xi} \tag{A.17}$$

Since the integrals (A.5, A.8, A.12, A.14 and A.16) that arise in this macrocrack/microcrack interaction formulation are integrated exactly, the accuracy of the crack interaction solution obtained using this method is limited only by the number of terms taken in the pseudo-traction series and the choice of collocation points.